

Surface magnetic anisotropy-mediated spin Hall magnetoresistance and spin Seebeck effects in a YIG/Pt heterostructure

V. Kalappattil^{a,*}, R. Das^b, M.H. Phan^a, and H. Srikanth^{a,*}

^aDepartment of Physics, University of South Florida, Tampa, Florida, 33620, United States

^bPhenikaa Research and Technology Institute (PRATI), A&A Green Phoenix Group, 167 Hoang Ngan, Hanoi 10000, Vietnam

The role of magnon-phonon coupling in the low-temperature behavior of the spin Seebeck effect (SSE) in YIG/Pt has been puzzling for more than a decade. To elucidate the origin of the anomalous peak around 80 K, we investigate the temperature evolution of SSE, spin Hall magnetoresistance (SMR), and magnetic anisotropy in the same YIG/Pt heterostructure. We find that these effects, along with magnetic damping, show the peaks at the same temperature (~80 K). This simultaneous occurrence, where no heat is applied in the case of SMR, rules out the phonon-magnon drag related origin of SSE in the YIG/Pt system. We further show that the intrinsic surface anisotropy behavior in YIG is responsible for controlling the SSE, SMR, and magnetic damping in the YIG/Pt structure. Our findings not only help to understand these effects fundamentally but also provide an effective way for improving them by manipulating the surface magnetic anisotropy for spin caloritronic applications.

Keywords: YIG; Magnetic anisotropy; Spin Seebeck Effect; spin Hall magneto-resistance

* Corresponding authors: vijaysankar8819@gmail.com; sharihar@usf.edu

1. Introduction

Spin-orbit coupling (SOC) has been found to be the reason behind many novel magnetic phenomena, especially in spintronics (Giant magneto-resistance, Anomalous Hall Effect, Spin Hall Effect, etc.), because it couples spin and charge of the electron [1-3]. The spin Hall effect (SHE) has attracted growing attention due to its potential application in spintronics [3-5]. In a nutshell, the SHE converts a charge current (J_C) to a spin current (J_S). The Onsager reciprocal of SHE is an inverse spin Hall effect (ISHE), which converts J_S into J_C [2,3]. It has been shown that the spin Seebeck effect (SSE) voltage is extracted using the ISHE voltage generated in a heavy metal [6]. When SHE and ISHE coexist in the same metal, it leads to a magneto-resistance, described as spin Hall magneto-resistance (SMR) [7-10]. When J_C is passing through a metal with a strong spin-orbit coupling (in most cases, Pt), as a result of the SHE, J_C is converted into J_S in which spin polarization vector, σ is parallel to the surface. When this spin current reaches the surface, it gets reflected back into the material, and during its backflow, it again gets converted into the charge current J_C by the ISHE. This charge current is now added to the original flow of the charge current. For instance, when a ferromagnetic insulator, YIG ($Y_3Fe_5O_{12}$), is coupled to Pt, the backflow of the spin current from the interface is controlled by the magnetization state in YIG. When σ is parallel to the magnetization M in YIG, the backflow of J_S is at maximum. However, when the angle between them changes, a portion of the spin current is absorbed as a spin-transfer torque (STT) in YIG. As a result, the resistance R becomes maximum when σ is perpendicular to M and minimum when σ is parallel to M . This change in resistance is referred to as SMR [7].

A theoretical model for SMR in a YIG/Pt system was proposed by Chen *et al.* [8]. However, this model has not reached a complete consensus on the low-temperature behavior in

the YIG/Pt system. The SMR was found to increase monotonically from ambient temperature to the Curie temperature ($T_C \sim 560$ K), while its different temperature dependence was reported at lower temperatures by other groups [11,12]. Meyer *et al.* [11] showed a continuous decrease in the SMR value from 300 K down to 10 K. This was somewhat surprising as the low thermal fluctuations could result in an increase of the SMR at low temperatures. This behavior was explained by extracting different parameters like spin diffusion length (λ), spin hall angle θ_{sh} , and spin mixing conductance (G) from the SMR data. While G and λ remained constant in the fits, θ_{sh} decreased continuously from 300 K to 10 K, and this was thought to be a main cause for the observed SMR behavior. At the same time, other studies showed that the SMR first increased with lowering the temperature from 300 K to 100 K, reached a peak value at about 80 K, and decreased with temperature. This behavior was explained by considering the temperature dependence of λ in Pt [12]. On the other hand, this model has assumed that the contributions from the temperature dependences of θ_{sh} and G are negligible. Spin relaxation in Pt is governed by Elliot- Yafet spin orbit scattering model [13,14]. But the Elliot-Yafet mechanism is a bulk effect rather than an interface effect, while the SMR characteristics are highly governed by the ferromagnet/normal metal (FM/NM) interface. Using this model to fit the SMR data, λ value was obtained to vary from 0.5 to 4 nm over the investigated temperature range (0-280 K). However, the Pt spin diffusion length, as reported in previous works, yielded values between 1.5 nm to 12 nm [13]. As a result, the fitted data of SMR using the Elliot-Yafet spin-orbit scattering model was off by a factor of 3 [12].

Like SMR, the temperature dependence of SSE in YIG/Pt also has received considerable attention over the years [15-17]. The low-temperature peak observed in experiments led to several theoretical predictions. Recently, with the help of transverse susceptibility studies, we

have shown that YIG has a distinct surface anisotropy that differs from bulk anisotropy and directly influences the SSE at low temperatures [15]. Further, we have demonstrated an efficient way to improve the SSE by tuning the surface magnetic anisotropy of YIG by depositing a thin layer of organic semiconductor C_{60} on the YIG surface [16,17]. The addition of C_{60} in between YIG and Pt leads to the enhancement of carrier density at Fermi level and the reduction of the surface magnetic anisotropy, resulting in a giant SSE. In this study, through a comprehensive analysis of the temperature dependence of SMR, SSE, and magnetic anisotropy of the same YIG (single crystal)/Pt, we have established the correlation between the SMR and SSE and their association with the effective magnetic anisotropy.

2. Experimental methods

Magnetic measurements were performed on a YIG single crystal sample of dimension $6*4*1 \text{ mm}^3$ grown by the floating zone method along the (111) direction. The YIG single crystal was purchased from Crystal Systems Corporation, Hokuto, Yamanashi, Japan. **After cleaning the polished surface of YIG with acetone and isopropyl alcohol (IPA), we deposited a Pt Hall bar on one side of the single crystal for SMR and the ~5nm Pt strip on the other side for SSE measurements. Pt was deposited using a shadow mask via DC magnetron sputtering. We used a custom-designed multifunctional transport insert, which is housed inside the PPMS for both SSE and SMR measurements. This gives us the capability to reach to 10 K with a maximum of the 7 T applied field.** Angle-dependent magneto resistance (ADMR) can be measured in the longitudinal or transverse direction. When the resistance is measured parallel to the charge current flow, it is called a longitudinal ADMR, and when it is perpendicular, it is termed as the transverse ADMR. Since our interest is in the temperature dependence of SMR, we will focus our discussion on the longitudinal ADMR measurements in the remaining sections. Fig. 1a

shows a schematic of the SMR measurement set-up. The schematic of the longitudinal SSE (LSSE) measurement is shown in Fig. 1b. For LSSE measurements, YIG/Pt was sandwiched between two copper plates. A polyamide film heater was attached to the bottom plate, and the top plate temperature was controlled through molybdenum screws attached to the cold finger of the cryostat. A temperature gradient of approximately 1 K was achieved by applying sufficient current to the heater module. K-type thermocouples and silicon diode sensors were used to monitor the temperature of the top and bottom plates. Temperature gradient was measured at each temperature, and the heater power was adjusted to maintain a 1 K gradient throughout the measurement. Details of the measurements can be found in [15]. In radio-frequency transverse susceptibility (RF TS) measurements, the sample was placed in an inductive coil, which is part of an ultra-stable, self-resonant tunnel-diode oscillator in which a perturbing small RF field ($H_{AC} \approx 10$ Oe) was applied perpendicular to the DC field [18-21]. The coil with the sample was inserted into the PPMS chamber, which provides temperature variation from 10 K to 350 K in the applied field up to 7 T.

It has been shown that the SMR of a NM/FM structure can be quantified using the equation [10],

$$\rho_{xx} = \rho + \rho_0 + \Delta\rho_1(1 - m_y^2), \quad (1)$$

where ρ is the bulk resistivity of the metal, and m_y is the component M

$$\frac{\Delta\rho}{\rho} = -\frac{\theta_{SH}^2 2\lambda}{d} \tanh \frac{d}{2\lambda}, \quad (2)$$

$$\frac{\Delta\rho_1}{\rho} \approx \frac{\theta_{SH}^2 \lambda}{d} 2\lambda G_r \frac{\tanh^2\left(\frac{d}{2\lambda}\right)}{\sigma + 2\lambda G_r \coth \frac{d}{N}}, \quad (3)$$

where θ_{SH} is the spin Hall angle, λ is the spin diffusion length, N is the metal thickness, and G_r is the real part of spin mixing conductance G .

The longitudinal ADMR can be approximated as

$$\frac{\Delta\rho_L}{\rho_0} = \frac{R_l(0^\circ) - R_l(90^\circ)}{R_{l_0}} \quad (4)$$

Figure 2 shows the resistance change obtained when an angle between the applied magnetic field and charge current, α , is 0 and 90 degrees. In both directions, the ADMR signal saturates approximately around 500 Oe, which is the saturating field for the YIG crystal from M - H measurements. As the applied magnetic field (H) was swept from positive to negative saturation, when H was parallel to J_C , a resistance increase was observed. Interestingly, below 300 Oe, we have observed a low field plateau as reported by Wu *et al.* [22], which is similar to the low field anomaly of SSE as shown in Fig. S1. In the case of SSE, this behavior has been attributed to the surface anisotropy being different from the bulk anisotropy of the YIG crystal [23]. This relationship also points out the role the surface magnetic anisotropy plays in controlling the SMR. In other words, the surface magnetic anisotropy of YIG may mediate both the SSE and SMR effects in a Pt/YIG system. To clarify this hypothesis, we have systematically studied the temperature dependences of SMR, SSE, and surface magnetic anisotropy field (H_S) of this system. ADMR measurements were performed at different temperatures from 20 to 300K, and the obtained result of $\frac{\Delta\rho_L}{\rho_0}(T)$ is shown in Fig. 3a. It can be clearly seen in this figure that with increasing temperature, the SMR amplitude first increased, reached a maximum value around 80 K, and finally decreased at higher temperatures.

Generating pure spin current via SSE has been realized in many systems over the years. When a FM/NM structure is subjected to the temperature gradient in the presence of a magnetic field, thermal injection of spin current occurs from FM to NM. When the NM has very high spin-orbit coupling, the injected spin current is converted into charge current via inverse spin Hall effect (ISHE). The spin current J_s can be expressed as [24,25],

$$J_s = \frac{G\gamma\hbar k_B \Delta T}{2\pi M_s V_a} \quad (5)$$

Where, where G is the spin mixing conductance, γ is the gyromagnetic ratio, \hbar is the reduced Planck constant, k_B is the Boltzmann constant, V_a is the magnetic coherence volume, M_s is the saturation magnetization, and ΔT is the temperature difference between magnons in FM and electrons in NM.

A typical SSE signal obtained for the Pt/YIG sample at 300 K and 100 K is shown in Fig. S1, and its temperature dependence down to 10 K is displayed in Fig. 3b. SSE value at 1.5 KOe is used in this plot. Similar to the previously reported behavior [26], the LSSE voltage (V_{LSSE}) increased as the temperature decreased from 300 to 80 K, and an opposite trend was observed at lower temperatures. A peak SSE voltage is obtained at ~80 K, as expected. SSE coefficient is defined as $S_{LSSE} = \left(\frac{V_{LSSE}}{L}\right) / \left(\frac{\Delta T}{t}\right)$, where L is the length and t is the thickness. As from this calculation, our S_{LSSE} value at room temperature is 3.25×10^{-7} V/K.

The temperature evolution of the surface magnetic anisotropy field of YIG is investigated using radio-frequency transverse susceptibility (TS). In the TS method, as the DC field is swept from positive saturation to negative saturation of the sample under study, the resonant frequency

of the coil with the sample changes proportionally to the transverse susceptibility of the sample, which is calculated using

$$\frac{\Delta\chi_T}{\chi_T} (\%) = \frac{|\chi_T(H) - \chi_T^{sat}|}{\chi_T^{sat}} \times 100 \quad (6)$$

It has been theoretically shown that a ferromagnetic material should yield TS peaks at the anisotropy fields ($\pm H_k$) and switching fields ($-H_S$) as the DC field is swept from positive to negative saturation and vice versa [18-21]. In the YIG/Pt structure, we have observed 4 different peaks from a full bipolar TS scan (see Fig. S2), indicating 2 different anisotropy states corresponding to the surface and bulk anisotropies of the system. In this study, we are interested in the surface magnetic anisotropy field (H_{KS}), and its temperature dependence is therefore shown in Fig. 3c. It is observed in this figure that with lowering the temperature, the H_{KS} first increased, reached a maximum around 80 K, and finally decreased. This temperature evolution of H_{KS} is in line with that of SMR and SSE.

3. Results and discussion

Figure 3d shows the temperature dependences of SSE, SMR, and surface anisotropy field (H_{KS}) on a normalized scale. We can divide the entire plot into two regions: (i) from 300 K to 80 K and (ii) 80 K to 10 K. In region (i), all three parameters tend to increase as we go from high to low temperature. However, the SSE and SMR show an exponential increase in this range while H_K follows a linear temperature dependence. This could be explained by the temperature dependence of the spin Hall angle (θ_{sh}) and spin diffusion length (λ) in Pt. Both parameters, along with the spin mixing conductance (G) are crucial in determining the obtained signals of the SSE and SMR. We expect G to be temperature independent or weakly dependent as compared to

the other two factors in this scenario. θ_{sh} , which is governed by the ratio of spin conductivity to Pt conductivity, could be temperature-dependent as reported by different groups [26,27]. Assuming the Elliot-Yafet model of spin relaxation in this system, λ is inversely proportional to the temperature, mainly due to the temperature dependence of phonon scattering [12]. Similar effects of these two parameters in SSE and SMR lead to the comparable exponential behavior in the region (i) as seen in Fig. 3d, a slight slope change in SSE around ~ 170 K is attributed to the spin reorientation that occurs in YIG at that temperature. **Due to the single ion anisotropy of Fe^{2+} ions present in YIG, the system undergoes a change in easy axis direction around 170 K [15].** At the same time, H_{KS} varies in this region as expected from a Stoner-Wohlfarth type behavior. However, as the temperature reached around 100 K, non-collinear magnetization between bulk and surface spins of YIG yielded a peak in anisotropy, which is directly reflected in both the SMR and SSE. In region (ii), all the three parameters (SSE, SMR, and H_{KS}) drop linearly with lowering the temperature below ~ 80 K. This stipulates less dominant roles of θ_{sh} and λ in this region as H_{KS} varies similarly even in the absence of Pt (the only difference is that H_{KS} peak value shifts depending upon the effect of the top layer on the surface).

Magnetic field dependences of SSE and SMR are given in Fig. S.3. We have observed a clear dependence of magnetic field on SSE compared to SMR. As mentioned in Ref. 26, this could be explained by the role of low-frequency magnons [26]. It is generally accepted that low-frequency magnons dominate SSE. At a higher magnetic field, these magnons are partially frozen, leading to a reduction in the SSE voltage. At the same time, magnon propagation length increases with decreasing temperature. Competition between these two factors causes a shift in the SSE peak to a higher temperature with a higher applied field. On the contrary, the SMR peak is mainly controlled by the surface magnetic property of the material, such as surface magnetic

anisotropy. After the saturation, an increase in the applied magnetic field does not affect the SMR values much. This is evident from the data shown in Fig. S2b.

In our previous study [15], we have shown that the low-temperature peak (80 K) can be attributed to the non-collinear magnetization between the surface and bulk of the YIG crystal. One of the supporting and motivational reasons for the study was the temperature difference between the peak in thermal conductivity and SSE in the case of YIG [26]. Very recently, another study has shown that, when the temperature is measured directly from the sample instead of taking it from the contact layers, the temperature gap between the thermal conductivity and SSE peak is reduced considerably [27]. With further analysis, Iguchi *et al.* have concluded that the pure thermal magnon theory of LSSE is not completely appropriate, and there is a need for looking back into the phonon-mediated magnon excitation theory. Our systematic study, as presented in this work, shows that similar to the SSE, the SMR also peaks at the same temperature (~80 K) along with the surface anisotropy field. Phonon-magnon drag, which has been a prominent mechanism proposed in the SSE theory due to the applied thermal gradient and its similarity with thermopower. The appearance of the SMR peak at the same temperature, where there is no temperature gradient, can rule out the possibility of phonon assistance for achieving higher SSE values. As shown by our transverse susceptibility studies, YIG possesses two different types of magnetic anisotropies corresponding to the bulk and surface magnetic states. The sharp decrease in H_{KS} below ~75 K can be attributed to the rotation of surface spins away from the perpendicular easy-axis direction. In a magnetic system like YIG, which is composed of two different surface and bulk spin configurations, this is very much possible. When the temperature dependence and alignment of these spin configurations are different, the low-temperature peak can be considered as the temperature where surface spins are rotated away

from bulk spins, like a spin canting phenomenon. This is also clear from the reduction of the total magnetization below 75 K in YIG [15]. This reduction in magnetization also directly contributes to the reduction in SSE and SMR and at low temperatures, as spin mixing conductance at the interface depends on the magnetization. *Guo et al.* have shown the thickness and top layer material dependences of the low-temperature SSE peak [26]. According to their study, the SSE peak shifted to the right as the thickness decreased. To further understand the effect, we have measured surface anisotropy in the YIG crystal (1 mm thick) and the 7 μ m thick YIG film, which are expected to show two different surface spin states corresponding to two different surface anisotropy fields. As shown in Fig. S4, there is a clear peak shift in magnetic anisotropy to high temperature in the case of 7 μ m YIG. A similar trend can also be found for the peak dependence of SSE on the top layer. As we have shown previously in reference 16, depositing a top layer such as C₆₀ has shifted the anisotropy peak to different temperatures, which once again is consistent with Fig. 4 in reference 26. These results confirm the role of surface over bulk magnetic properties in controlling the thermo-spin-transport effects.

Furthermore, we note the results reported by Flaig *et al.* [28] and Jermain *et al.* [29] about the temperature dependence of magnetic damping in YIG. The linear increases of the Gilbert damping parameter and the full width at half maximum (FWHM) linewidth from 300 to 100 K have been explained well by the theories of Kasuya and Lecraw [30] and later modified by Cherepanov *et al.* [31]. However, both the theories failed to interpret the temperature dependence of these parameters below 100 K; the experimental results have shown a low-temperature peak in linewidth measured in a constant field. The theories also failed to accommodate the shift in the peak points with higher frequency. Both these experimental deviations have been explained using impurity concentration in the YIG sample. Relaxation

mechanisms with impurities could be much different from that of pure YIG, and this may lead to the different behavior at low temperatures. Nevertheless, difficulties in obtaining modeling parameters for the impurities have raised several questions about these methods, and a proper consensus cannot be reached. Our findings, as reported in this study, can lend insight into the low-temperature Gilbert damping behavior, similar to that of the SSE and SMR. Non-collinear magnetization dynamics and different temperature responses between bulk and surface spins of YIG can cause a spin-canting behavior and a different surface anisotropy as compared to bulk anisotropy. Changes in anisotropy possibly excite more spin waves, similar to the recently observed voltage-controlled magnetic anisotropy (VCMA) excitation of spin waves in ferromagnetic metals [32]. The relation between resonant frequency and anisotropy field is given by [28],

$$f_{r_{110}} = \frac{\gamma}{2\pi} \mu_0 (H_{\text{applied}} + H_K)$$

$$f_{r_{440}} = \frac{\gamma}{2\pi} \mu_0 \left(H_{\text{applied}} + H_K + \frac{M_s}{9} \right),$$

where $f_{r_{110}}$ and $f_{r_{440}}$ are the resonant frequencies for mode 110 and 440, respectively, γ is the gyromagnetic ratio, H_{applied} is the applied electric field, and H_K is the magnetic anisotropy field. The shift in linewidth with frequency can also be understood from these results. However, more microscopic analysis and models are required to fully understand the relaxation mechanisms in this system.

4. Conclusions

In summary, we have observed the similar temperature dependence of SSE and SMR in the YIG/Pt structure, with their maximal values achieved at the same temperature of ~80 K.

Since the SSE and SMR are of completely different microscopic origins, the presence of the same peak pinpoints an intrinsic characteristic of the YIG sample. TS studies on the same sample have also shown a similar peak in the temperature dependence of H_{KS} . We can thus relate the low-temperature behavior of these effects to a non-collinear alignment of bulk and surface spin states in YIG. These results can be extended to explain the low-temperature Gilbert damping and FWHM linewidth behavior in the same system. These important findings allow us to conclude that there are material-dependent origins rather than the phenomenon-dependent origin, and the existing theoretical models should be adjusted to explain these microscopic behaviors. Since YIG is one of the most interesting ferrimagnetic insulators for spintronics, a clear understanding of the different bulk and surface anisotropies and their effects on the spintronic phenomena will have a significant impact on the materials design and application perspectives.

CRedit Authorship Contribution Statement:

V. Kalappattil - Conceptualization, Data curation, Formal analysis, Investigation, Methodology, Validation, Visualization, Writing - original draft. R. Das - Conceptualization, Data curation, Investigation, Writing - review & editing, M.H. Phan - Supervision, Project administration, Writing - review & editing. H. Srikanth - Supervision, Project administration, Writing - review & editing.

Declaration of Competing Interest:

The authors declare that they have no known competing financial interests or personal relationships that could have appeared to influence the work reported in this paper.

Acknowledgements:

Research at the University of South Florida was supported by the U.S. Department of Energy, Office of Basic Energy Sciences, Division of Materials Sciences and Engineering under Award No. DE-FG02-07ER46438.

Data Availability:

The data that support the findings of this study are available from the corresponding author upon reasonable request.

References

1. N. Nagaosa, J. Sinova, S. Onoda, A. H. MacDonald, and N. P. Ong, *Rev. Mod. Phys.* **82** (2010) 1539.
2. J. Sinova, S. O. Valenzuela, J. Wunderlich, C. H. Back, and T. Jungwirth, *Rev. Mod. Phys.* **87** (2015) 1213.
3. G. Vignale, *J. Supercond. Novel Magn.* **23**, (2010) 3.
4. T. Jungwirth, J. Wunderlich, and K. Olejník, *Nature Mater.* **11**, (2012) 382.
5. X. Kou, Y. Fan, and K. L. Wang, *J. Phys. Chem. Solids* **128**, (2019) pp. 2–23..
6. K. Uchida, S. Takahashi, K. Harii, J. Ieda, W. Koshibae, K. Ando, S. Maekawa, and E. Saitoh, *Nature (London)* **455**, (2008) 778.
7. H. Nakayama, M. Althammer, Y.-T. Chen, K. Uchida, Y. Kajiwara, D. Kikuchi, T. Ohtani, S. Geprägs, M. Opel, S. Takahashi, R. Gross, G. E. W. Bauer, S. T. B. Goennenwein, and E. Saitoh, *Phys. Rev. Lett.* **110** (2013) 206601.
8. Y. T. Chen, S. Takahashi, H. Nakayama, M. Althammer, S. T. B. Goennenwein, E. Saitoh, and Gerrit E. W. Bauer, *Phys. Rev. B* **87** (2013) 144411.
9. M. Isasa, A. Bedoya-Pinto, S. Vélez, F. Golmar, F. Sanchez, L. E. Hueso, J. Fontcuberta, and F. Casanova, *Appl. Phys. Lett.* **105** (2014) 142402.
10. X.-P. Zhang, F. S. Bergeret, and V. N. Golovach, *Nano Lett.* **19** (2019) 6330.
11. S. Meyer, M. Althammer, S. Geprägs, M. Opel, R. Gross, and S. T. B. Goennenwein,, *Appl. Phys. Lett.* **104** (2014) 242411.
12. S. R. Marmion, M. Ali, M. McLaren, D. A. Williams, and B. J. Hickey, *Phys. Rev. B* **89** (2014) 220404(R).
13. L. Q. Liu, R. A. Buhrman, and D. C. Ralph, arXiv:1111.3702 (2011).

14. J. Fabian, and S. D. Sarma, *J. Vac. Sci. Tech. B* **17**, (1999) 1708.
15. Kalappattil V, Das R, Phan M.H and Srikanth H, *Sci. Rep* **7** (2017) 13316.
16. V. Kalappattil, R. Geng, R. Das, H. Luong, M. Pham, T. Nguyen, A. Popescu, L. M. Woods, M. Klau, H. Srikanth, M. H. Phan, *Mater. Horiz.* **7** (2020) 1413.
17. R. Das, V. Kalappattil, R. Geng, H. Luong, M. Pham, T. Nguyen, T. Liu, M. Wu, M. H. Phan, and H. Srikanth, *AIP Adv.* **8** (2018) 055906.
18. H. Srikanth, J. Wiggins, H. Rees, *Review of Scientific Instruments* **70** (1999) 3097–3101.
19. N. A. Frey Huls, N. S. Bingham, M. H. Phan, H. Srikanth, D. D. Stauffer, and C. Leighton, *Phys. Rev. B* **83** (2011) 024406.
20. A. Aharoni, E. H. Frei, S. Shtrikman, and D. Treves, *Bull. Res. Counc. Isr., Sect. F* **6A** (1957) 215.
21. D. Cimpoesu, A. Stancu, L. Spinu, *Phys. Rev. B* **76** (2007) 054409.
22. P. H. Wu and S. Y. Huang, *Phys. Rev. B* **94** (2016) 024405.
23. K. Uchida, J. Ohe, T. Kikkawa, S. Daimon, D. Hou, Z. Qiu, and E. Saitoh, *Phys. Rev. B* **92** (2015) 014415.
24. J. Xiao, G. E. W. Bauer, K. C. Uchida, E. Saitoh, and S. Maekawa, *Phys. Rev. B* **81**, (2010) 214418.
25. M. Weiler, M. Althammer, M. Schreier, J. Lotze, M. Pernpeintner, S. Meyer, H. Huebl, R. Gross, A. Kamra, J. Xiao, Y. T. Chen, H. Jiao, G. E. W. Bauer and S. T. B. Goennenwein, *Phys. Rev. Lett.*, **111**, (2013) 176601.
26. E. Guo, J. Cramer, A. Kehlberger, C. A. Ferguson, D. A. MacLaren, G. Jakob, and M. Kläui, *Phys. Rev. X* **6** (2016) 031012.
27. R. Iguchi, K. Uchida, S. Daimon, and E. Saitoh, *Phys. Rev. B* **95** (2017) 174401.

28. H. Maier-Flaig, S. Klingler, C. Dubs, O. Surzhenko, R. Gross, M. Weiler, H. Huebl, and S. T. B. Goennenwein, *Phys. Rev. B* **95** (2017) 214423.
29. C. L. Jermain, S. V. Aradhya, N. D. Reynolds, R. A. Buhrman, J. T. Brangham, M. R. Page, P. C. Hammel, F. Y. Yang, and D. C. Ralph, *Phys. Rev. B* **95**, (2017) 174411.
30. T. Kasuya and R. C. LeCraw, *Phys. Rev. Lett.* **6** (1961) 223.
31. V. Cherepanov, I. Kolokolov, and V. L'vov, *Phys. Rep.* **229** (1993) 81.
32. R. Verba, M. Carpentieri, G. Finocchio, V. Tiberkevich and A. Slavin, *Sci. Report* **7** (2016) 25018.

Figure captions:

Fig. 1 Measurement geometry for (a) Longitudinal Angle dependent magnetoresistance (ADMR), (b) Longitudinal SSE, and (c) TS measurement set up.

Fig. 2 Longitudinal SMR changes when the applied magnetic field (H) is (a) parallel and (b) perpendicular to charge current J_c (α is 0° and 90°); (c) shows the compiled plot.

Fig. 3 Temperature dependence of SMR, SSE and H_{KS} for the YIG/Pt system.

Fig. 1

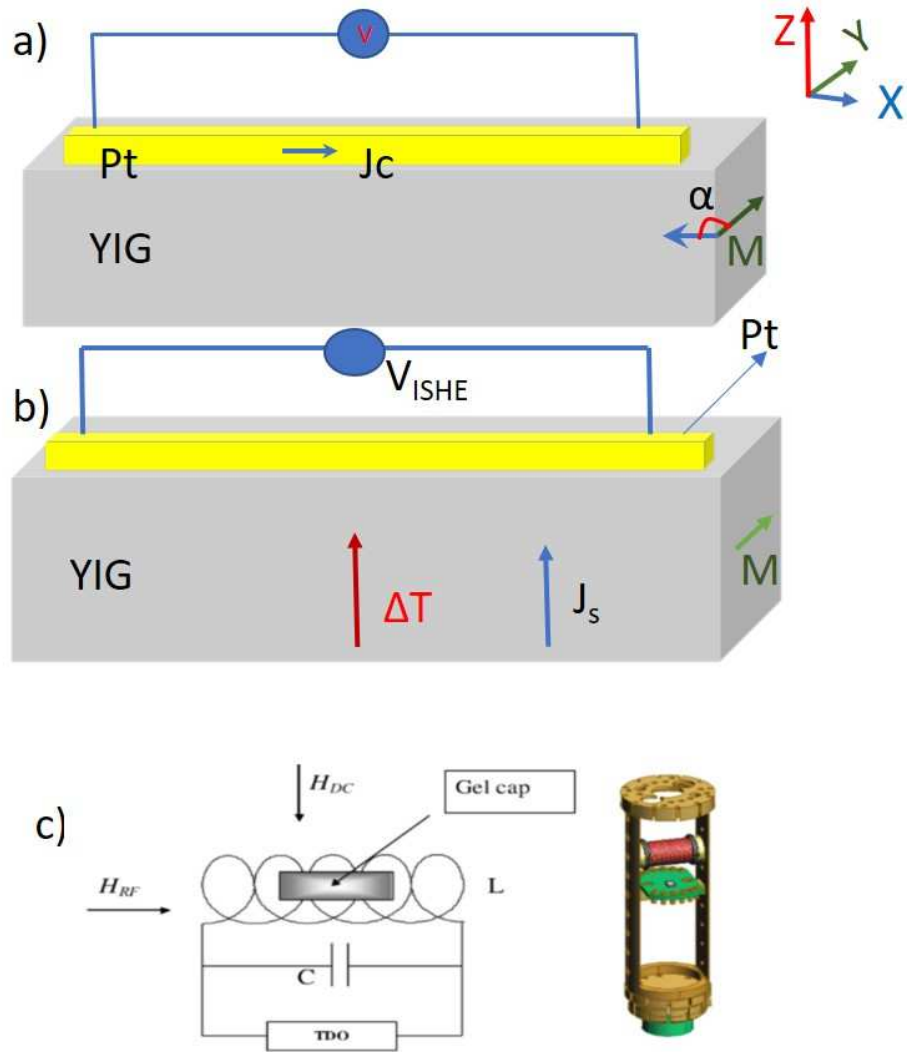


Fig. 2

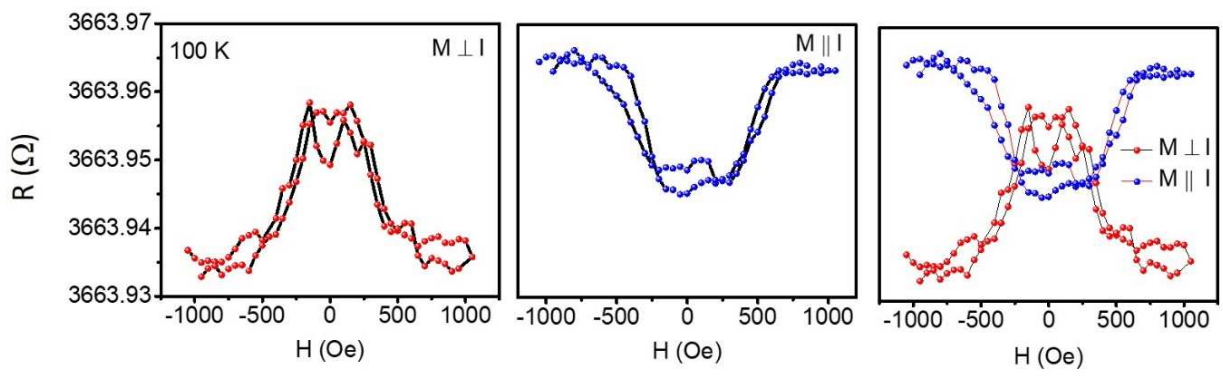


Fig. 3

